HHS Public Access

Author manuscript

Appl Surf Sci. Author manuscript; available in PMC 2022 December 30.

Published in final edited form as:

Appl Surf Sci. 2021 December 30; 570: . doi:10.1016/j.apsusc.2021.151163.

Manganese-containing Bioactive Glass Enhances Osteogenic Activity of TiO_2 Nanotube Arrays

Roberta M. Sabino[1], **Julietta V. Rau**[2,3], **Angela De Bonis**[4], **Adriana De Stefanis**[5], **Mariangela Curcio**[4], **Roberto Teghil**[4], **Ketul C. Popat**[1,6,7,*]

[1]School of Advanced Materials Discovery, Colorado State University, Fort Collins, USA

[2]Istituto di Struttura della Materia, Consiglio Nazionale delle Ricerche (ISM-CNR), Via del Fosso del Cavaliere 100, 00133 Rome, Italy

[3]I.M. Sechenov First Moscow State Medical University, Institute of Pharmacy, Department of Analytical, Physical and Colloid Chemistry, Trubetskaya 8, build. 2, 119991 Moscow, Russia

[4]Dipartimento di Scienze, Università della Basilicata, Via dell'Ateneo Lucano, 10-85100 Potenza, Italy

[5]Istituto di Struttura della Materia, Consiglio Nazionale delle Ricerche (ISM-CNR), Montelibretti Unit, Via Salaria km 29.300, 00015 Monterotondo Scalo, Italy

[6]School of Biomedical Engineering, Colorado State University, Fort Collins, USA

[7]Department of Mechanical Engineering, Colorado State University, Fort Collins, USA

Abstract

Titanium and its alloys are the most used biomaterials for orthopedic and dental applications. However, up to 10% of these medical devices still fail, mostly due to implant loosening and suboptimal integration at the implant site. The biomaterial surface plays a critical role in promoting osseointegration, which can reduce the risk of device failure. In this study, we propose a novel surface modification on titanium to improve osteogenic differentiation by depositing manganese-containing bioactive glass (BG) on TiO_2 nanotube arrays. The surfaces were characterized by scanning electron microscopy, energy dispersive X-ray spectrometer, contact angle goniometry, and X-ray photoelectron spectroscopy. Cell toxicity, viability, adhesion, and proliferation of adipose-derived stem cells on the surfaces were investigated up to 7 days. To evaluate the osteogenic properties of the surfaces, alkaline phosphatase activity, total protein, osteocalcin expression, and calcium deposition were quantified up to 28 days. The results indicate

*Author of correspondence: Ketul C. Popat (ketul.popat@colostate.edu).

Credit Author Statement

Roberta Maia Sabino: Methodology, Validation, Formal Analysis, Investigation, Data Curation, Writing - Original Draft

Ketul C. Popat: Conceptualization, Writing - Review & Editing, Supervision, Project Administration, Funding Acquisition

Declaration of interests

The authors declare that they have no known competing financial interests or personal relationships that could have appeared to influence the work reported in this paper.

that TiO_2 nanotube arrays modified with BG promote cell growth and induce increased osteocalcin and calcium contents when compared to unmodified TiO_2 nanotube arrays. The deposition of manganese-containing bioactive glass onto TiO_2 nanotubes demonstrates the ability to enhance osteogenic activity on titanium, showing great potential for use in orthopedic and dental implants.

Graphical abstract

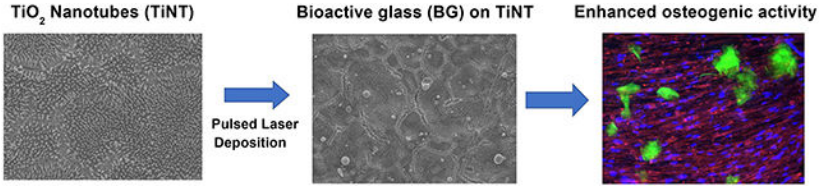

Keywords

Orthopedic implants; Osteogenic differentiation; TiO_2 nanotubes; Bioactive glass; Manganese

1. INTRODUCTION

Titanium-based implants are widely employed in orthopedics and dentistry due to their outstanding mechanical and biocompatible properties [1]. In addition to its high strength, moderate Young's modulus and low density, titanium also shows enhanced resistance to corrosion, which makes it gold standard biomaterial for orthopedic implants [2]. However, the native oxide layer present on titanium-based surfaces is responsible for their bio-inertness and poor wear resistance, which often leads to failure of these implants [3,4]. It is well established that the surface properties of medical devices play a critical role in the osseointegration process and, consequently, in the long-term implant life [5,6]. To improve the cell interaction with the biomaterial and enhance bone healing, various surface modification techniques are being investigated on titanium, such as acid-etching, anodization, plasma spraying, and bioactive coatings, which includes the incorporation of biomolecules, biopolymers, or bioactive glasses [7-9].

Bioactive glass ceramic coatings have recently attracted considerable attention in regenerative medicine due to their capacity to promote bone repair, wound healing, and drug delivery [10,11]. Silica-based bioactive glass is a promising material for orthopedic implants as the weak Si-O bond present on its structure makes it possible to bind with natural bone [10]. Silicon is also considered to stimulate the differentiation of osteoblasts and participate in the early stages of bone matrix formation [12]. In addition, the bioactive glass can have its composition easily modified by incorporation of different elements, which can be used to modulate the cellular response. Previous study has shown that a novel manganese-containing bioactive glass ceramic material significantly improves adipogenic, chondrogenic, osteogenic, and antimicrobial properties [13]. Manganese (Mn) is an essential cofactor for many enzymes and is vital for the formation of bone matrix [14]. It has been shown that Mn-containing bioactive glass has the ability to foster cell adhesion and improve bone mineralization [15,16].

Nanotopographical structures are another approach to enhance bone formation and osseointegration of the implants [17]. The nanoscale topography has shown to control protein adsorption and improve bone cell growth and differentiation due to the structural similarity to the bone tissue nanostructure [18]. Emerging fabrication techniques led to development of different nanostructured titanium surfaces such as nanofibers, nanotubes, and nanopores for orthopedic and dental applications [19-21]. TiO_2 nanotube arrays exhibit higher cell viability and alkaline phosphatase activity, and increased calcium deposition in comparison with bare titanium surfaces, suggesting a favorable template for osteogenic differentiation [8,22]. Despite these recent advances, none of the proposed surface modifications have proved sufficient for assuring optimal osseointegration. Therefore, there is an urgent need to develop surfaces that improve the osteogenic activity of titanium, thus preventing device failure and the need for revision surgeries. It has been demonstrated that the combination of surface nanotopography with a bioactive agent can have a synergistic effect for enhancing the implant osseointegration [23,24].

In this work, a combined approach was employed to design a novel titanium surface with enhanced osteogenic differentiation by using nanotopography and bioactive glass coating. TiO_2 nanotube arrays were fabricated via anodization process to modify the surface topography of titanium. Then, Mn-containing bioactive glass (BG) was deposited onto TiO_2 nanotubes using Pulsed Laser Deposition (PLD). The surfaces were characterized by scanning electron microscopy (SEM), energy dispersive X-ray spectrometer (EDS), contact angle goniometry, and X-ray photoelectron spectroscopy (XPS). Adipose-derived stem cells (ADSCs) were cultured on the substrates, and their cytotoxicity, viability, adhesion, and proliferation were investigated after 1, 4 and 7 days. Osteogenesis was then induced, and the osteogenic properties was evaluated via alkaline phosphatase (ALP) activity, total protein, osteocalcin expression, and calcium concentration assays after 14 and 28 days of cell culture.

2. MATERIALS AND METHODS

2.1 Fabrication of TiO_2 nanotube arrays with Mn-containing bioactive glass (BG)

TiO_2 nanotube arrays were fabricated by an anodization technique previously reported [25]. In summary, the titanium was cleaned with acetone, M90 detergent, isopropanol, and deionized (DI) water. Platinum foil was utilized as the cathode, and titanium foil was utilized as the anode. The electrolyte solution was prepared by mixing 95% v/v diethylene glycol (Alfa), 3% v/v DI water, and 2% v/v hydrofluoric acid (Alfa). The anodization process was performed at 55 V for 22 hrs, with further annealing at 530 °C for 3 hrs.

The Na_2O-K_2O-MgO-MnO-CaO-CaF_2-P_2O_5-SiO_2 glass ceramic was prepared by a sol-gel process as described elsewhere and is composed of amorphous calcium phosphate and crystalline wollastonite and fluorapatite phases [13]. Mn-containing bioactive glass (BG) was deposited on TiO_2 nanotube arrays using a Pulsed Laser Deposition (PLD) set up consisting of a Nd:YAG laser source (Handy YAG, Quanta System, λ = 532 nm, pulse duration = 7 ns, repetition rate = 10 Hz) and a stainless steel chamber with a high vacuum pumping equipment (scroll and turbomolecular, 10^{-4} Pa), a rotating target holder and a heating substrate holder. The laser beam was focused at 45° on the target by a 350 mm

quartz focusing lens. Suitable deposition conditions were chosen varying target-substrate distance and number of laser pulses. All films were deposited at room temperature, setting the substrate parallel to the target at a distance of 3 cm and for a deposition time of 1 hr. The fluence was kept at 12 J/cm^2, as optimized in our previous work [13]. The following notation will be used in this paper: unmodified TiO_2 nanotube arrays: TiNT; Mn-containing bioactive glass deposited onto TiO_2 nanotube arrays: BG-TiNT.

2.2 Surface characterization

The surface morphology of the substrates was characterized using scanning electron microscopy (SEM, JEOL 6500). Before imaging at 15 kV accelerating voltage, the substrates were gold coated (10 nm). The elemental analysis of BG-TiNT surface was performed by energy dispersive X-ray spectrometer (EDS) using the same equipment at 20 kV accelerating voltage.

The wettability of the substrates was measured using a Ramé-Hart Model 250 goniometer and images were obtained via DROPimage advanced software. Approximately 8 μl of DI water was placed on the substrates to measure the static contact angles.

The surface chemistry of the substrates was investigate using X-ray photoelectron spectroscopy (XPS, ESCA Systems Spectrometer 5800). XPS analysis was conducted at 15 kV with a takeoff angle of 45°. Survey spectra were collected from 0 to 1100 eV, and the elemental composition was determined using MultiPak software.

2.3 Cell culture

Human adipose-derived stem cells (ADSCs) were isolated from adipose tissue by Prof. Cox-York lab from Colorado State University. The procedures were conducted in compliance with the National Institutes of Health's “Guiding Principles for Ethical Research”. ADSCs at passage 4 were cultured in growth media (α-MEM, HyClone™) with 10% (v/v) Fetal Bovine Serum and 1% (v/v) penicillin/streptomycin at 37 °C and 5% CO_2 [26]. Prior to cell seeding, the substrates were sterilized via incubation in 70% ethanol for 15 mins, followed by three rinses with PBS and exposure to UV light for 30 mins. ADSCs were then inoculated on the substrates at a concentration of 10,000 cells/ml and incubated at 37°C and 5% CO_2 until further studies.

2.4 Cell toxicity and viability

The cytotoxicity of the substrates was characterized via a lactate dehydrogenase (LDH) assay (Pierce). After 1 day of cell culture, 50 μl of substrates-exposed growth media was mixed with 50 μl of LDH reaction solution and incubated at 37°C. After 30 mins, 50 μl of stop solution was added, and the absorbance was measured at 490 nm and 680 nm using a microplate reader (FLUOstar Omega) [27]. The maximum LDH release was obtained by adding 10% (v/v) Triton X-100 to wells without any substrates to promote cell lysis. Spontaneous LDH release was obtained in the wells where cells were not exposed to the substrates. The cytotoxicity was calculated following the manufacturer's guidelines.

The cell viability on the substrates was evaluated via an Alamar Blue assay (Invitrogen). After 4 and 7 days of cell culture, the substrates were incubated in culture media with 10% of assay reagent at 37 °C for 6 hrs. After this incubation period, the absorbance of the resulting solutions was measured at 570 and 600 nm by a microplate reader [28]. The Alamar Blue reduction percentage correlates with the activity of viable cells and it was calculated as described by the manufacturer protocol. The ADSCs were also seeded in empty wells (positive control), while the negative control was carried out only with the media without cells. The results obtained for the negative control was used to eliminate the influence of the cell media on the Alamar Blue reduction percentage. The cell viability outcomes obtained for the substrates were normalized using the results from the positive control [29].

2.5 Cell adhesion and proliferation

The cell adhesion and proliferation on the substrates were examined using fluorescence microscopy. After 4 and 7 days, the cells found adhering to the substrates were fixed by incubation in 3.7% formaldehyde solution in PBS for 15 mins, with three subsequent rinses with PBS (5 mins each). The cells were then permeabilized in 1% Triton X-100 solution in PBS for 3 mins, followed by twofold rinse with PBS [30]. After that, the substrates were placed in rhodamine phalloidin solution (70 nM, Cytoskeleton) for 20 mins, followed by 5 mins incubation in DAPI stain solution (300 nM, ThermoFisher Scientific) in a dark environment. After rinsing with PBS, the substrates were imaged using a fluorescence microscope (Zeiss). The number of cells on the substrates was obtained by counting the stained nuclei using ImageJ software.

The cell morphology on the substrates was characterized after 4 and 7 days using SEM as detailed elsewhere [31]. In summary, the substrates were placed in a fixative solution composed of glutaraldehyde, sodium cacodylate and sucrose for 40 mins. After that, the substrates were moved to a buffer solution (fixative with no glutaraldehyde) for 10 mins. The substrates were dehydrated by exposure to ethanol solutions for 10 mins each step [31]. Then, the substrates were incubated in 100% hexamethyldisilazane for 10 mins. After HMDS removal, the substrates were dried and imaged using SEM as described in Section 2.2.

2.6 Osteogenic activity

After 7 days of cell culture on the substrates, osteogenesis was induced using a supplemented media. This media was prepared by adding 50 μg/mL of ascorbic acid, 10^{-8} M dexamethasone, and 6 mM β-glycerol phosphate to the growth media and it was changed every other day for 21 days.

After 14 and 28 days of cell culture (i.e., 7 and 21 days after using supplemented media), the substrates were rinsed once with PBS and moved to new wells. Then, the substrates were incubated in Triton X-100 (0.2% v/v in DI water) for 20 mins at 100 rpm to remove all protein content from the substrates. The supernatant was then stored in the freezer for further Micro BCA and ALP activity assays.

A Micro BCA assay kit (Thermo Scientific) was used to quantify the total amount of protein content on the substrates. 150 μL of supernatant (0.2% Triton X-100 solution with protein extracted) was mixed with 150 μL of working reagent and incubated for 2 hrs at 37 °C in dark environment, followed by the measurement of absorbance at 562 nm. The results for the total amount of protein was determined via a standard absorbance curve obtained previously using the manufacturer's guidelines [18].

A colorimetric assay kit (QuantiChrom™, BioAssay Systems) was used to determine the ALP activity on the substrates. 50 μL of the supernatant (0.2% Triton X-100 solution with protein extracted) was mixed with 150 μL of working reagent. The absorbance was measured at 405 nm after 0 and 4 mins and the ALP activity was obtained following the manufacturer's guidelines. The ALP activity was normalized to total protein content on each substrate [32].

The osteocalcin expression by the cells on the substrates was investigated via immunofluorescent staining. After 14 and 28 days of cell culture, the cells found adhering to the substrates were fixed and permeabilized as described in Section 2.5. Then, the substrates were placed in bovine serum albumin (BSA) solution (10% v/v in PBS) for 30 mins to block nonspecific binding sites. After that, the substrates were incubated with osteocalcin primary antibody solution (1:100 in 1% BSA) for 60 mins, followed by three rinses with PBS. The substrates were then placed in secondary antibody-FITC solution (1:200 in 1% BSA) for 45 mins. After rinsing with PBS, the substrates were stained with DAPI and rhodamine phalloidin and imaged as detailed in Section 2.5. The osteocalcin expression on each substrate was obtained by calculating the percentage osteocalcin area via ImageJ software [33].

The calcium deposition on the substrates was determined by a calcium reagent set (Teco Diagnostics). After supernatant removal, the substrates were dried and incubated in 6 N HCl solution for 2 hrs to dissolve the deposited calcium. After that, 20 μl of the acid-calcium solution was collected from each well and mixed with 1 ml of working reagent prepared following the manufacturer’s protocol. The absorbance of the acid-calcium solution was read at 570 nm and the calcium concentration was calculated using the manufacturer's guidelines. The calcium concentration was normalized to total protein content on each substrate [18].

The cell morphology and mineral deposition on the substrates were also investigated by SEM. After 14 and 28 days of cell culture, the substrates were fixed and dehydrated as detailed in Section 2.5. The imaging was conducted as outlined in Section 2.2.

2.7 Statistical analysis

SEM images, EDS and XPS analysis were reconfirmed on at least 2 different samples of each surface. Contact angle measurements were carried out on at least 3 different samples of each surface ($n_{min} = 3$). All *in vitro* studies were performed with $n_{min} = 3$ for qualitative analyses and $n_{min} = 5$ for quantitative analyses. The quantitative results were statistically analyzed using ANOVA and Tukey tests at a 5 % significance level using GraphPad Prism software.

3. RESULTS AND DISCUSSION

Insufficient osseointegration is the main reason for failure of dental and orthopedic prostheses. Titanium-based materials have been largely used for decades for these implants, however their intrinsic bio-inertness is still a challenge for rapid and successful osseointegration [34]. Several techniques are being investigated on titanium to enhance its osteogenic activity, such as acid-etching, hydrothermal treatment, and bioactive coatings; however, there is still a need to develop implant surfaces that integrate better with the bone tissue [35]. In this work, we designed a novel titanium surface to promote osteogenic differentiation of ADSCs by combining bioactive glass with nanotopography. First, titanium was anodized to form TiO_2 nanotubes using HF solution, and the nanotubes formation is provoked by a field-assisted dissolution process [25].

A thin film of bioactive glass was deposited by means of nanosecond PLD. This technique allows to deposit films well adherent to the substrate, retaining the target stoichiometry. During the interaction of a nanosecond laser pulse with a solid target, the heating of the target surface takes place with its melting and evaporation. In the few ns after the laser shot, it has been observed the formation of a neutral plasma composed of ions, atoms, electrons, and droplets. The hot expanding plasma arrests on the substrate surface where the coating grows by gas condensation and droplets coalescence mechanisms [36,37]. The nano and micro roughness of bioactive films deposited by nanosecond PLD could be beneficial for biomedical applications.

After fabrication, the substrates were characterized by SEM, EDS, contact angle measurements, and XPS. ADSCs toxicity, viability, adhesion, and proliferation were investigated after 1, 4, and 7 days of cell culture. To characterize the osteogenic properties of the substrates, the osteogenic differentiation of ADSCs was evaluated via alkaline phosphatase activity, total protein, osteocalcin expression, and calcium concentration assays after 14 and 28 days *in vitro*.

3.1 Surface characterization

The surface morphology of TiNT and BG-TiNT was imaged using SEM (Fig. 1). Both surfaces display uniform and vertically oriented nanotubes. SEM results demonstrate that the deposition of Mn-containing bioactive glass does not change the nanotubes' topography, however, deposits accumulated on some regions of the surface are visible. Maintaining the nanoscale morphology is desired due to the enhanced biocompatibility and ability to form bone *in vitro* and *in vivo* [38,39]. The nanotopography on biomaterial surfaces is responsible for bio mimicking the bone tissue and imparts better microenvironments for cell anchorage, growth, and bone formation [40]. It has been shown that TiO_2 nanotube arrays, in comparison with smooth titanium, improve bone cell growth and differentiation, as well as reduce immune response and bacterial adhesion [8,22,41,42]. Therefore, in this study, TiO_2 nanotube arrays was used as control instead of bare titanium.

The elemental composition of BG-TiNT surface was analysed using EDS (Fig. 2a). The spectra revealed the presence of Si, F, Ca, Na, Mg, P, and Mn, demonstrating the successful deposition of Mn-containing bioactive glass on TiO_2 nanotube arrays. In addition, the

mapping analysis show the homogeneous distribution of these elements on the surface, indicating that the nanoparticles of BG are uniformly distributed on TiNT surface (Fig. 2b, 2c).

The wettability of TiNT and BG-TiNT was instigated by measuring the apparent contact angle (θ) using DI water (Fig. 3). The wettability is important as it influences the biological response of the material, such as cell adhesion and spreading [43]. The results indicate that TiNT is superhydrophilic (i. e., when $\theta < 10°$), while BG-TiNT is hydrophilic (when $\theta < 90°$) [44]. As expected, TiNT is superhydrophilic because of the oxide layer present on its surface and increased roughness [45]. Previous study has also demonstrated the hydrophilic nature of BG material [11]. Researchers have observed that hydrophilic surfaces tend to improve cell attachment and spreading in comparison with hydrophobic surfaces [46,47]. In addition, implant surfaces with contact angle between 35° and 80° is desired as extremely hydrophilic biomaterials tend to inhibit cell-cell interactions [48,49]. Fig. 3 shows that the contact angle of BG-TiNT falls in this desired range, showing moderate hydrophilicity,

The surface chemistry of TiNT and BG-TiNT was characterized using XPS (Fig. 4). Survey scans show peaks for Ti2p, O1s, and C1s for both substrates. As expected, BG-TiNT shows the presence of F1s, Ca2p, Si2p. Mg2p, Na1s, P2s, and Mn2p peaks, which are characteristics of the bioactive glass composition. The presence of C1s was due to the impurities on the surfaces and in the XPS chamber. The intensity of Ti2p peak is lower on BG-TiNT when compared to TiNT and this is due to the deposition of the bioactive glass. The XPS results agree with EDS analysis, showing the successful deposition of the BG on TiO_2 nanotube arrays.

3.2 Cell toxicity and viability

Stem cells have shown to be a great cell source for studies in tissue engineering and regenerative medicine [33]. Different types of stem cells can be used to investigate the osteogenic properties of biomaterials such as bone marrow-derived mesenchymal stem cells (MSCs) and adipose-derived stem cells (ADSCs) [22]. Both cells exhibit pluripotency in vitro, being able to differentiate into osteoblasts and with similar potential for osteogenic differentiation [50]. However, in contrast with MSCs, ADSCs harvesting is noninvasive, with minimal donor-site morbidity. In addition, ADSCs have attracted considerable attention recently due their improved accessibility and high yield rate [32]. Therefore, in this work, ADSCs were used to study the cell response and osteogenic activity of the designed surfaces.

The cytotoxicity of the substrates was investigated after 1 day of ADSCs culture using LDH assay (Fig. 5a). The LDH enzyme is released from cells when apoptosis or necrosis happen, thus being a marker of cell membrane integrity [51]. The cytotoxicity of TiNT and BG-TiNT substrates was determined by considering the maximum and spontaneous LDH releases. The maximum LDH release was obtained by lysing all the cells, and spontaneous LDH release was obtained for the cells in the wells and not exposed to the substrates. According to ISO 10993-5, a biomaterial is considered cytotoxic if cytotoxicity values are greater than 10% [27]. Previous works have proved that TiO_2 nanotube arrays are not cytotoxic and exhibit good biocompatibility [4,52,53]; however the cytotoxicity of BG-TiNT has not yet

been investigated. The results indicate that both substrates show cytotoxicity less than 10%, with no significant difference between them. Therefore, the deposition of Mn-containing bioactive glass on the TiO_2 nanotube arrays does not cause any cytotoxic effects to the cells.

The cell viability on the substrates was evaluated after 4 and 7 days of ADSCs culture using Alamar Blue assay (Fig. 5b). The metabolically active cells react with resazurin present in the Alamar Blue reagent, reducing it to resorufin by the dehydrogenase enzymes [27]. Therefore, a higher Alamar Blue reduction indicates more viable cells on the substrates. The results show that, after 4 days of cell culture, there is no significant difference in cell viability. After 7 days, TiNT presents significant higher cell viability when compared to BG-TiNT; however, both substrates promoted considerable cell viability when compared to positive control (100% cell viability) after 7 days.

3.3 Cell adhesion and proliferation

The cell adhesion and proliferation on the substrates were investigated after 4 and 7 days of ADSCs culture using fluorescence microscopy. This initial cell attachment and proliferation are critical as it affects differentiation into bone cells and the implant long-term stability. The results indicate that both substrates promote considerable cell adhesion and proliferation (Fig. 6a). The number of cells adhered was obtained by counting the stained nuclei using ImageJ software. Fig. 6b shows that there was no significant difference in the number of adhered cells between substrates after 4 and 7 days, although BG-TiNT exhibits higher cell adhesion than TiNT. These results are in contrast with the ones from cell viability, indicating that both substrates foster similar cell growth.

The cell morphology on the substrates was characterized using SEM (Fig. 6c). The results show a higher degree of cell spreading on BG-TiNT on day 4 and 7 when compared to TiNT. Although the number of cells found adhering to the substrates were not significantly different after 7 days, BG-TiNT shows a higher spread, which influences the late cell behaviors such as growth and differentiation [54]. This ability for facilitating cell spreading is due to the bioactive glass composition as the presence of Mn ions is responsible for promoting cell proliferation and differentiation [13].

3.4 Osteogenic activity

After 7 days of cell culture on the substrates, osteogenesis was induced using a supplemented media. Ascorbic acid, dexamethasone, and β-glycerol phosphate were added to the media to promote collagen type I secretion, RUNX2 transcription factor activity, and a source of phosphate, respectively [55]. Osteogenesis was induced to guarantee the differentiation would happen on both substrates concurrently, thus being able to compare how cells behave on them. The osteogenic activity of biomaterials is crucial as it is responsible for the implant osseointegration and its long-term stability.

After 14 and 28 days of cell culture, the ALP production on the substrates was investigated. ALP is an enzyme responsible for converting organophosphate to inorganic phosphate and its activity is a biochemical marker at the early stage of cell differentiation [6]. Fig. 7 indicates there was no significant difference in ALP activity between substrates after 14 days. However, after 28 days, TiNT shows significant higher ALP activity in comparison

with BG-TiNT. Since ALP activity oscillates during the differentiation and mineralization processes, it could be possible that its peak for BG-TiNT happened before 28 days [56]. In addition, the substantial rise in ALP activity on both substrates between day 14 and day 28 indicates that the cells are differentiating into osteoblasts [57].

The osteocalcin expression on the substrates was analyzed using immunofluorescent staining (Fig. 8a). Osteocalcin is a noncollagenous protein secreted by mature osteoblast cells and is responsible for promoting bone mineralization [33]. Therefore, osteocalcin is considered a late marker of differentiation. The results show no significant difference in osteocalcin area after 14 days (Fig. 8b). After 28 days, BG-TiNT shows significant higher percentage area coverage of osteocalcin when compared to TiNT. This was expected as the silicon presented in the bioactive glass nanoparticles is responsible to stimulate differentiation of bone cells and the synthesis of collagen type I due to its capacity to bond to hard tissue [58]. In addition, the presence of Mn is crucial to foster bone mineralization as it participates in the synthesis of glycosyltransferases and chondroitin sulfate that are involved in bone matrix formation [59]. It has been shown that Mn improve osteogenesis on titanium surfaces and, with its deficiency, osteoblast activity is impaired which can cause bone deformation [60]. In our previous work [13], it was found that Mn-containing BG favored the equine adipose tissue mesenchymal stem cells differentiation in adipogenic, chondrogenic and osteogenic lineages, being the latter qualitatively more pronounced. The detailed information on Si^{2+}, Ca^{2+} and Mn^{2+} ion kinetics can be found there. The results showed a significantly smaller amount of Mn^{2+} ions released in comparison with Si^{2+} and Ca^{2+} ions, with the release of silicon ions being the highest. In addition, the release of Mn^{2+} shows a slower rate compared to the other two ions. This could be explained due to the higher amount of SiO_2 and the smaller amount of Mn present in the bioactive glass composition. This is desired since excess in exposure to Mn can cause toxic effects [61]. Previous studies have investigated the isolated effects of different ions in cell behavior and osteogenic activity [15,62]. It has been shown that Mn^{2+} ions are able to improve cell proliferation and induce high levels of ALP activity, while Si^{2+} stimulate the differentiation of osteoblasts and Ca^{2+} promotes bone mineralization [58,62,63]. Therefore, a synergistic effect on the release of Mn^{2+}, Si^{2+} and Ca^{2+} ions is responsible for the improvement of the osteogenic activity. The osteocalcin results also suggest that the ALP peak for BG-TiNT happened before 28 days due to higher content of osteocalcin, which is a late marker of differentiation.

The calcium deposition on the substrates was also quantified after 14 and 28 days of cell culture. It is worth noting that, although BG already has calcium in its composition, this calcium content does not interfere with this assay, since it is not free to react with HCl. To confirm that, the assay was performed on BG-TiNT before the cell culture, and the outcome was zero. After the increase in ALP activity and protein production, the next step in bone matrix formation is the mineralization [22]. Mineralization is the process responsible for hydroxyapatite production, made of phosphorus and calcium. Fig. 9 indicates no significant difference in calcium concentration after 14 days of cell culture. After 28 days, BG-TiNT presents significant higher calcium deposition when compared to TiNT. This is consistent with osteocalcin results as higher osteocalcin expression is responsible for improved bone mineralization and calcium deposition.

The cell morphology and mineral deposition on the substrates were also investigated by SEM after 14 and 28 days of cell culture (Fig. 10). After 14 days, ADSCs on both substrates are spreading, with no visual evidence of mineralization, which indicates that the cells are still differentiating [64]. However, after 28 days, TiNT and BG-TiNT are all covered by cells. The results also show some mineral deposits after 28 days (blue circles). SEM images agree with osteocalcin and calcium results, since BG-TiNT shows more mineral deposits than TiNT, indicating enhanced osteogenic response of BG-TiNT.

4. CONCLUSIONS

In this study, TiO_2 nanotube arrays (TiNT) were successfully modified with manganese-containing bioactive glass (BG) via pulsed laser deposition to improve their osteogenic properties. Results show that BG nanoparticles are homogeneously distributed on the surface and that the deposition of BG does not change the nanotubes' topography. Cell toxicity, viability, adhesion, and proliferation studies show that BG-TiNT is not toxic and promote considerable cell attachment and proliferation. Osteogenic activity outcomes also show that BG-TiNT enhanced osteogenic differentiation of ADSCs, with increased mineral deposition, osteocalcin expression, and calcium concentration in comparison with TiNT. The silicon presented in BG nanoparticles is responsible to stimulate differentiation of osteoblast cells and is involved in the early stages of bone matrix formation. In addition, the presence of manganese ions is crucial for improving cell growth and bone mineralization. Therefore, the modified titanium surface provides a prospective material with good osteogenic potential which may improve the implant osseointegration and reduce the risk of device failure.

ACKNOWLEDGEMENTS

Research reported in this publication was supported by National Heart, Lung and Blood Institute of the National Institutes of Health under award number R01HL135505 and R21HL139208. The authors thank Prof. Kimberly Cox-York from Colorado State University for generously donating the ADSCs.

REFERENCES

[1]. He M, Chen X, Cheng K, Weng W, Wang H, Enhanced Osteogenic Activity of TiO2 Nanorod Films with Microscaled Distribution of Zn-CaP, ACS Appl. Mater. Interfaces8 (2016) 6944–6952. doi:10.1021/acsami.6b01284. [PubMed: 26930577]

[2]. Li J, Mutreja I, Tredinnick S, Jermy M, Hooper GJ, Woodfield TBF, Hydrodynamic control of titania nanotube formation on Ti-6Al-4V alloys enhances osteogenic differentiation of human mesenchymal stromal cells, Mater. Sci. Eng. C109 (2020) 110562. doi:10.1016/j.msec.2019.110562.

[3]. Shin YC, Pang KM, Han DW, Lee KH, Ha YC, Park JW, Kim B, Kim D, Lee JH, Enhanced osteogenic differentiation of human mesenchymal stem cells on Ti surfaces with electrochemical nanopattern formation, Mater. Sci. Eng. C99 (2019) 1174–1181. doi:10.1016/j.msec.2019.02.039.

[4]. Cowden K, Dias-Netipanyj MF, Popat KC, Adhesion and Proliferation of Human Adipose-Derived Stem Cells on Titania Nanotube Surfaces, Regen. Eng. Transl. Med5 (2019) 435–445. doi:10.1007/s40883-019-00091-9.

[5]. Calvo-Guirado JL, Satorres-Nieto M, Aguilar-Salvatierra A, Delgado-Ruiz RA, Maté-Sánchez de Val JE, Gargallo-Albiol J, Gómez-Moreno G, Romanos GE, Influence of surface treatment on osseointegration of dental implants: histological, histomorphometric and radiological analysis in vivo, Clin. Oral Investig19 (2015) 509–517. doi:10.1007/s00784-014-1241-2.

[6]. Liu K, Zhang H, Lu M, Liu L, Yan Y, Chu Z, Ge Y, Wang T, Tang C, Enhanced bioactive and osteogenic activities of titanium by modification with phytic acid and calcium hydroxide, Appl. Surf. Sci478 (2019) 162–175. doi:10.1016/j.apsusc.2019.01.219.

[7]. Dai G, Wan W, Chen J, Wu J, Shuai X, Wang Y, Enhanced osteogenic differentiation of MC3T3-E1 on rhBMP-2 immobilized titanium surface through polymer-mediated electrostatic interaction, Appl. Surf. Sci471 (2019) 986–998. doi:10.1016/j.apsusc.2018.11.243.

[8]. Popat KC, Leoni L, Grimes CA, Desai TA, Influence of engineered titania nanotubular surfaces on bone cells, Biomaterials. 28 (2007) 3188–3197. doi:10.1016/J.BIOMATERIALS.2007.03.020. [PubMed: 17449092]

[9]. Wang C, Hu H, Li Z, Shen Y, Xu Y, Zhang G, Zeng X, Deng J, Zhao S, Ren T, Zhang Y, Enhanced Osseointegration of Titanium Alloy Implants with Laser Microgrooved Surfaces and Graphene Oxide Coating, ACS Appl. Mater. Interfaces11 (2019) 39470–39483. doi:10.1021/acsami.9b12733. [PubMed: 31594306]

[10]. Arango-Ospina M, Nawaza Q, Boccaccini AR, Silicate-based nanoceramics in regenerative medicine, in: Nanostructured Biomater. Regen. Med, Elsevier, 2019: pp. 255–273. doi:10.1016/B978-0-08-102594-9.00009-7.

[11]. Rau JV, Curcio M, Raucci MG, Barbaro K, Fasolino I, Teghil R, Ambrosio L, De Bonis A, Boccaccini AR, Cu-Releasing Bioactive Glass Coatings and Their in Vitro Properties, ACS Appl. Mater. Interfaces11 (2019) 5812–5820. doi:10.1021/acsami.8b19082. [PubMed: 30653295]

[12]. Henstock JR, Canham LT, Anderson SI, Silicon: The evolution of its use in biomaterials, Acta Biomater. 11 (2015) 17–26. doi:10.1016/j.actbio.2014.09.025. [PubMed: 25246311]

[13]. Rau JV, De Stefanis A, Barbaro K, Fosca M, Yankova VG, Matassa R, Nottola SA, Nawaz Q, Ali MS, Peukert W, Boccaccini AR, Adipogenic, chondrogenic, osteogenic, and antimicrobial features of glass ceramic material supplemented with manganese, J. Non. Cryst. Solids559(2021) 120709. doi:10.1016/j.jnoncrysol.2021.120709.

[14]. Wu T, Shi H, Liang Y, Lu T, Lin Z, Ye J, Improving osteogenesis of calcium phosphate bone cement by incorporating with manganese doped β-tricalcium phosphate, Mater. Sci. Eng. C109 (2020) 110481. doi:10.1016/j.msec.2019.110481.

[15]. Nawaz Q, Rehman MAU, Burkovski A, Schmidt J, Beltrán AM, Shahid A, Alber NK, Peukert W, Boccaccini AR, Synthesis and characterization of manganese containing mesoporous bioactive glass nanoparticles for biomedical applications, J. Mater. Sci. Mater. Med29 (2018) 64. doi:10.1007/s10856-018-6070-4. [PubMed: 29737411]

[16]. Rocha Barrioni B, Oliveira AC, De Fá Tima Leite M, De Magalhã Es Pereira M, Solgel-derived manganese-releasing bioactive glass as a therapeutic approach for bone tissue engineering, J Mater Sci. 52 (2017) 8904–8927. doi:10.1007/s10853-017-0944-6.

[17]. Kaur M, Singh K, Review on titanium and titanium based alloys as biomaterials for orthopaedic applications, Mater. Sci. Eng. C102 (2019) 844–862. doi:10.1016/J.MSEC.2019.04.064.

[18]. Sabino RM, Mondini G, Kipper MJ, Martins AF, Popat KC, Tanfloc/heparin polyelectrolyte multilayers improve osteogenic differentiation of adipose-derived stem cells on titania nanotube surfaces, Carbohydr. Polym251 (2021) 117079. doi:10.1016/j.carbpol.2020.117079. [PubMed: 33142622]

[19]. Sabino RM, Kauk K, Madruga LYC, Kipper MJ, Martins AF, Popat KC, Enhanced hemocompatibility and antibacterial activity on titania nanotubes with tanfloc/heparin polyelectrolyte multilayers, J. Biomed. Mater. Res. - Part A108 (2020) 992–1005. doi:10.1002/jbm.a.36876.

[20]. Manivasagam VK, Popat KC, In Vitro Investigation of Hemocompatibility of Hydrothermally Treated Titanium and Titanium Alloy Surfaces, ACS Omega. (2020). doi:10.1021/acsomega.0c00281.

[21]. Kolen'ko YV, Kovnir KA, Gavrilov AI, Garshev AV, Frantti J, Lebedev OI, Churagulov BR, Van Tendeloo G, Yoshimura M, Hydrothermal synthesis and characterization of nanorods of various titanates and titanium dioxide, J. Phys. Chem. B110 (2006) 4030–4038. doi:10.1021/jp055687u. [PubMed: 16509693]

[22]. Cowden K, Dias-Netipanyj MF, Popat KC, Effects of titania nanotube surfaces on osteogenic differentiation of human adipose-derived stem cells, Nanomedicine Nanotechnology, Biol. Med17 (2019) 380–390. doi:10.1016/J.NANO.2019.01.008.

[23]. Zhang W, Wang G, Liu Y, Zhao X, Zou D, Zhu C, Jin Y, Huang Q, Sun J, Liu X, Jiang X, Zreiqat H, The synergistic effect of hierarchical micro/nano-topography and bioactive ions for enhanced osseointegration, Biomaterials. 34 (2013) 3184–3195. doi:10.1016/j.biomaterials.2013.01.008. [PubMed: 23380352]

[24]. Zhao P, Liu Y, Li T, Zhou Y, Leeflang S, Chen L, Wu C, Zhou J, Huan Z, 3D printed titanium scaffolds with ordered TiO2 nanotubular surface and mesoporous bioactive glass for bone repair, Prog. Nat. Sci. Mater. Int30 (2020) 502–509. doi:10.1016/j.pnsc.2020.08.009.

[25]. Sabino RM, Kauk K, Movafaghi S, Kota A, Popat KC, Interaction of blood plasma proteins with superhemophobic titania nanotube surfaces, Nanomedicine Nanotechnology, Biol. Med21 (2019). doi:10.1016/j.nano.2019.102046.

[26]. Plath AMS, Facchi SP, Souza PR, Sabino RM, Corradini E, Muniz EC, Popat KC, Filho LC, Kipper MJ, Martins AF, Zein supports scaffolding capacity toward mammalian cells and bactericidal and antiadhesive properties on poly(ɛ-caprolactone)/zein electrospun fibers, Mater. Today Chem20 (2021) 100465. doi:10.1016/j.mtchem.2021.100465.

[27]. Madruga LYC, Sabino RM, Santos ECG, Popat KC, de C. Balaban R, Kipper MJ, Carboxymethyl-kappa-carrageenan: A study of biocompatibility, antioxidant and antibacterial activities, Int. J. Biol. Macromol152 (2020) 483–491. doi:10.1016/j.ijbiomac.2020.02.274. [PubMed: 32109473]

[28]. Rufato KB, Souza PR, de Oliveira AC, Berton SBR, Sabino RM, Muniz EC, Popat KC, Radovanovic E, Kipper MJ, Martins AF, Antimicrobial and cytocompatible chitosan, N,N,N-trimethyl chitosan, and tanfloc-based polyelectrolyte multilayers on gellan gum films, Int. J. Biol. Macromol (2021). doi:10.1016/j.ijbiomac.2021.04.138.

[29]. de Almeida DA, Sabino RM, Souza PR, Bonafé EG, Venter SAS, Popat KC, Martins AF, Monteiro JP, Pectin-capped gold nanoparticles synthesis in-situ for producing durable, cytocompatible, and superabsorbent hydrogel composites with chitosan, Int. J. Biol. Macromol147 (2020). doi:10.1016/j.ijbiomac.2020.01.058.

[30]. Martins AF, Facchi SP, da Câmara PCF, Camargo SEA, Camargo CHR, Popat KC, Kipper MJ, Novel poly(ɛ-caprolactone)/amino-functionalized tannin electrospun membranes as scaffolds for tissue engineering, J. Colloid Interface Sci525 (2018) 21–30. doi:10.1016/J.JCIS.2018.04.060. [PubMed: 29680300]

[31]. da Câmara PCF, Madruga LYC, Sabino RM, Vlcek J, Balaban RC, Popat KC, Martins AF, Kipper MJ, Polyelectrolyte multilayers containing a tannin derivative polyphenol improve blood compatibility through interactions with platelets and serum proteins, Mater. Sci. Eng. C112 (2020) 110919. doi:10.1016/j.msec.2020.110919.

[32]. Bombaldi de Souza RF, Bombaldi de Souza FC, Thorpe A, Mantovani D, Popat KC, Moraes ÂM, Phosphorylation of chitosan to improve osteoinduction of chitosan/xanthan-based scaffolds for periosteal tissue engineering, Int. J. Biol. Macromol143 (2020) 619–632. doi:10.1016/J.IJBIOMAC.2019.12.004. [PubMed: 31811849]

[33]. Madruga LYC, Balaban RC, Popat KC, Kipper MJ, Biocompatible Crosslinked Nanofibers of Poly(Vinyl Alcohol)/Carboxymethyl-Kappa-Carrageenan Produced by a Green Process, Macromol. Biosci21 (2021) 2000292. doi:10.1002/mabi.202000292.

[34]. Zhang Y, Wang K, Song Y, Feng E, Dong K, Han Y, Lu T, Ca substitution of Sr in Sr-doped TiO2 nanotube film on Ti surface for enhanced osteogenic activity, Appl. Surf. Sci528 (2020) 147055. doi:10.1016/j.apsusc.2020.147055.

[35]. Manivasagam VK, Popat KC, Hydrothermally treated titanium surfaces for enhanced osteogenic differentiation of adipose derived stem cells, Mater. Sci. Eng. C128 (2021) 112315. doi:10.1016/J.MSEC.2021.112315.

[36]. De Bonis A, Curcio M, Fosca M, Cacciotti I, Santagata A, Teghil R, Rau JV, RBP1 bioactive glass-ceramic films obtained by Pulsed Laser Deposition, Mater. Lett175 (2016) 195–198. doi:10.1016/j.matlet.2016.04.044.

[37]. Curcio M, Rau JV, Santagata A, Teghil R, Laureti S, De Bonis A, Laser synthesis of iron nanoparticle for Fe doped hydroxyapatite coatings, Mater. Chem. Phys225 (2019) 365–370. doi:10.1016/j.matchemphys.2018.12.099.

[38]. Rasouli R, Barhoum A, Uludag H, A review of nanostructured surfaces and materials for dental implants: Surface coating, patterning and functionalization for improved performance, Biomater. Sci6 (2018) 1312–1338. doi:10.1039/c8bm00021b. [PubMed: 29744496]

[39]. Cheng Y, Yang H, Yang Y, Huang J, Wu K, Chen Z, Wang X, Lin C, Lai Y, Progress in TiO2 nanotube coatings for biomedical applications: A review, J. Mater. Chem. B6 (2018) 1862–1886. doi:10.1039/c8tb00149a. [PubMed: 32254353]

[40]. Hameed P, Manivasagam VK, Sankar M, Popat KC, Manivasagam G, Nanofibers and Nanosurfaces, in: Springer, Singapore, 2021: pp. 107–130. doi:10.1007/978-981-33-6252-9_4.

[41]. Bartlet K, Movafaghi S, Dasi LP, Kota AK, Popat KC, Antibacterial activity on superhydrophobic titania nanotube arrays, Colloids Surfaces B Biointerfaces. 166 (2018) 179–186. doi:10.1016/J.COLSURFB.2018.03.019. [PubMed: 29579729]

[42]. Smith BS, Capellato P, Kelley S, Gonzalez-Juarrero M, Popat KC, Reduced in vitro immune response on titania nanotube arrays compared to titanium surface, Biomater. Sci1 (2013) 322–332. doi:10.1039/c2bm00079b. [PubMed: 32481857]

[43]. Mokhtari H, Ghasemi Z, Kharaziha M, Karimzadeh F, Alihosseini F, Chitosan-58S bioactive glass nanocomposite coatings on TiO 2 nanotube: Structural and biological properties, Appl. Surf. Sci441 (2018) 138–149. doi:10.1016/j.apsusc.2018.01.314.

[44]. Wang W, Lockwood K, Boyd LM, Davidson MD, Movafaghi S, Vahabi H, Khetani SR, Kota AK, Superhydrophobic Coatings with Edible Materials, ACS Appl. Mater. Interfaces8 (2016) 18664–18668. doi:10.1021/acsami.6b06958. [PubMed: 27403590]

[45]. Movafaghi S, Leszczak V, Wang W, Sorkin JA, Dasi LP, Popat KC, Kota AK, Hemocompatibility of Superhemophobic Titania Surfaces", Adv. Healthc. Mater (2017). doi:10.1002/adhm.201700647.

[46]. Webb K, Hlady V, Tresco PA, Relative importance of surface wettability and charged functional groups on NIH 3T3 fibroblast attachment, spreading, and cytoskeletal organization, J. Biomed. Mater. Res41 (1998) 422–430. doi:10.1002/(SICI)1097-4636(19980905)41:3<422::AID-JBM12>3.0.CO;2-K. [PubMed: 9659612]

[47]. Iuliano DJ, Saavedra SS, Truskey GA, Effect of the conformation and orientation of adsorbed fibronectin on endothelial cell spreading and the strength of adhesion, J. Biomed. Mater. Res27 (1993) 1103–1113. doi:10.1002/jbm.820270816. [PubMed: 8408123]

[48]. Menzies KL, Jones L, The impact of contact angle on the biocompatibility of biomaterials, Optom. Vis. Sci87 (2010) 387–399. doi:10.1097/OPX.0b013e3181da863e. [PubMed: 20375749]

[49]. Bumgardner JD, Wiser R, Elder SH, Jouett R, Yang Y, Ong JL, Contact angle, protein adsorption and osteoblast precursor cell attachment to chitosan coatings bonded to titanium, J. Biomater. Sci. Polym. Ed14 (2003) 1401–1409. doi:10.1163/156856203322599734. [PubMed: 14870943]

[50]. Zheng D, Neoh KG, Kang ET, Bifunctional coating based on carboxymethyl chitosan with stable conjugated alkaline phosphatase for inhibiting bacterial adhesion and promoting osteogenic differentiation on titanium, Appl. Surf. Sci360 (2016) 86–97. doi:10.1016/j.apsusc.2015.11.003.

[51]. Leszczak V, Popat KC, Improved in Vitro Blood Compatibility of Polycaprolactone Nanowire Surfaces, (n.d.). doi:10.1021/am503508r.

[52]. Simon-Walker R, Romero R, Staver JM, Zang Y, Reynolds MM, Popat KC, Kipper MJ, Glycocalyx-inspired nitric oxide-releasing surfaces reduce platelet adhesion and activation on titanium, ACS Biomater. Sci. Eng3 (2017) 68–77. doi:10.1021/acsbiomaterials.6b00572. [PubMed: 33429688]

[53]. Smith BS, Yoriya S, Grissom L, Grimes CA, Popat KC, Hemocompatibility of titania nanotube arrays, J. Biomed. Mater. Res. - Part A95 A (2010) 350–360. doi:10.1002/jbm.a.32853.

[54]. Liu WF, Chen CS, Engineering biomaterials to control cell function, Mater. Today8 (2005) 28–35. doi:10.1016/S1369-7021(05)71222-0.

[55]. Langenbach F, Handschel J, Effects of dexamethasone, ascorbic acid and β-glycerophosphate on the osteogenic differentiation of stem cells in vitro, Stem Cell Res. Ther4(2013) 117. doi:10.1186/scrt328. [PubMed: 24073831]

[56]. Fedarko NS, Bianco P, Vetter U, Robey PG, Human bone cell enzyme expression and cellular heterogeneity: Correlation of alkaline phosphatase enzyme activity with cell cycle, J. Cell. Physiol144 (1990) 115–121. doi:10.1002/jcp.1041440115. [PubMed: 2365738]

[57]. Wigmosta TB, Popat KC, Kipper MJ, Bone morphogenetic protein-2 delivery from polyelectrolyte multilayers enhances osteogenic activity on nanostructured titania, J. Biomed. Mater. Res. - Part A (2020). doi:10.1002/jbm.a.37109.

[58]. Hoppe A, Boccaccini AR, Biological Impact of Bioactive Glasses and Their Dissolution Products, Front. Oral Biol17 (2015) 22–32. doi:10.1159/000381690. [PubMed: 26201273]

[59]. Deng C, Yao Q, Feng C, Li J, Wang L, Cheng G, Shi M, Chen L, Chang J, Wu C, 3D Printing of Bilineage Constructive Biomaterials for Bone and Cartilage Regeneration, Adv. Funct. Mater27 (2017) 1703117. doi:10.1002/adfm.201703117.

[60]. Zhang X, Lv Y, Shan F, Wu Y, Lu X, Peng Z, Liu B, Yang L, Dong Z, Microstructure, corrosion resistance, osteogenic activity and antibacterial capability of Mn-incorporated TiO2 coating, Appl. Surf. Sci531 (2020) 147399. doi:10.1016/j.apsusc.2020.147399.

[61]. Aschner M, Guilarte TR, Schneider JS, Zheng W, Manganese: Recent advances in understanding its transport and neurotoxicity, Toxicol. Appl. Pharmacol221 (2007) 131–147. doi:10.1016/J.TAAP.2007.03.001. [PubMed: 17466353]

[62]. da Silva LM, dos S. Tavares D, dos S. Santos EA, Isolating the Effects of Mg^{2+}, Mn^{2+} and Sr^{2+} Ions on Osteoblast Behavior from those Caused by Hydroxyapatite Transformation, Mater. Res23 (2020) 20200083. doi:10.1590/1980-5373-MR-2020-0083.

[63]. An S, Gao Y, Ling J, Wei X, Xiao Y, Calcium ions promote osteogenic differentiation and mineralization of human dental pulp cells: implications for pulp capping materials, (n.d.). doi:10.1007/s10856-011-4531-0.

[64]. Anderson HC, Matrix vesicles and calcification., Curr. Rheumatol. Rep5 (2003) 222–226. doi:10.1007/s11926-003-0071-z. [PubMed: 12744815]

HIGHLIGHTS

- Mn-doped BG was deposited on TiO_2 nanotube arrays via pulsed laser deposition
- BG nanoparticles are homogeneously distributed on TiO_2 nanotube surface
- BG-TiO_2 nanotube arrays promote cell growth and induce increased differentiation

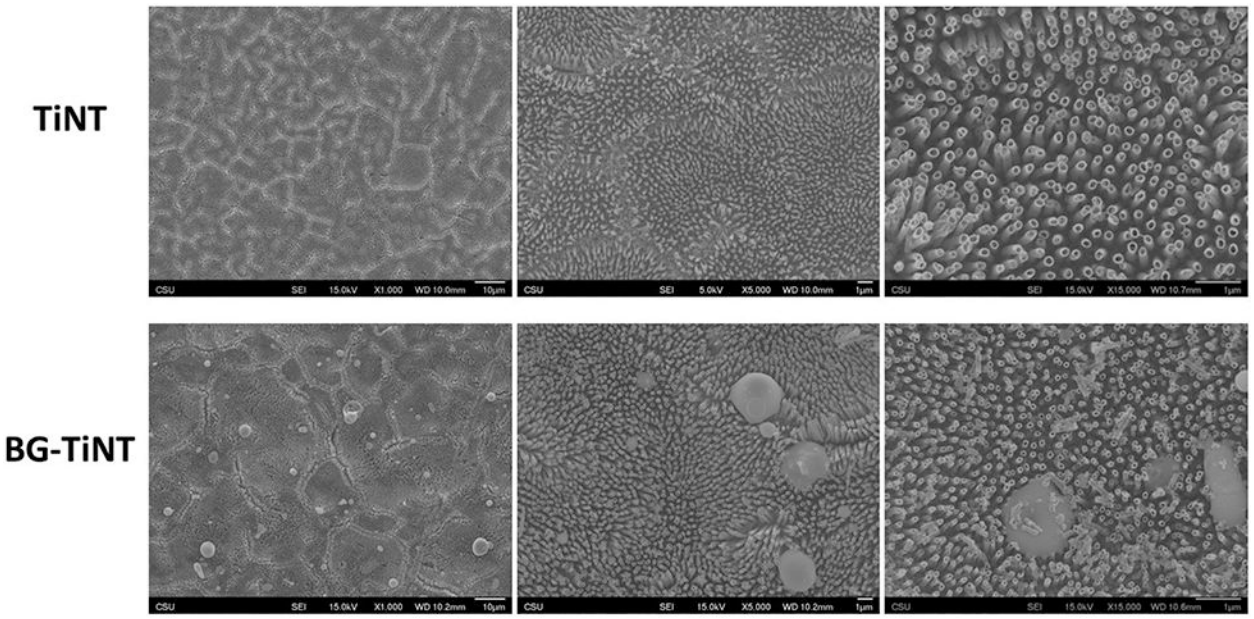

Fig. 1.
SEM images of TiNT and BG-TiNT. The images were taken at 1,000X, 5,000X, and 15,000X magnification.

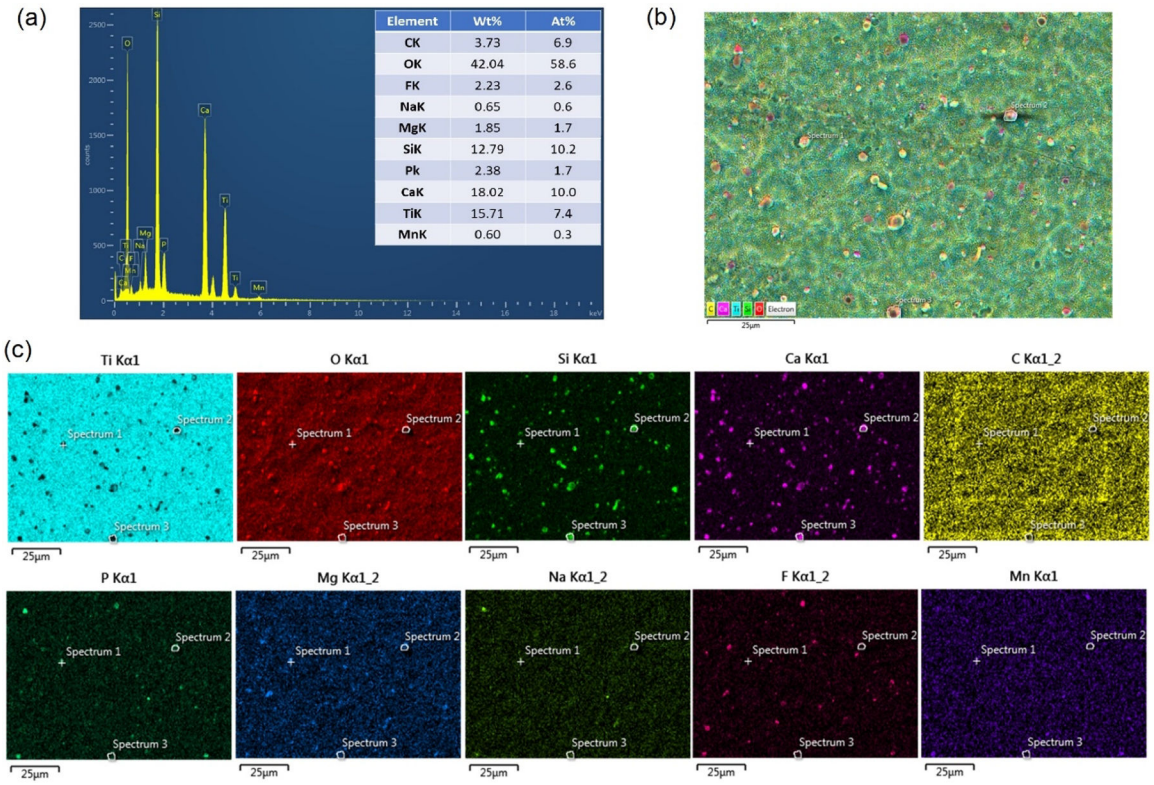

Fig. 2.

(a) EDS compositional analysis of BG-TiNT. (b) map in false colors of the selected zone. (c) Ti, O, Si, Ca, C, P, Mg, Na, F, Mn distrbution, respectivately.

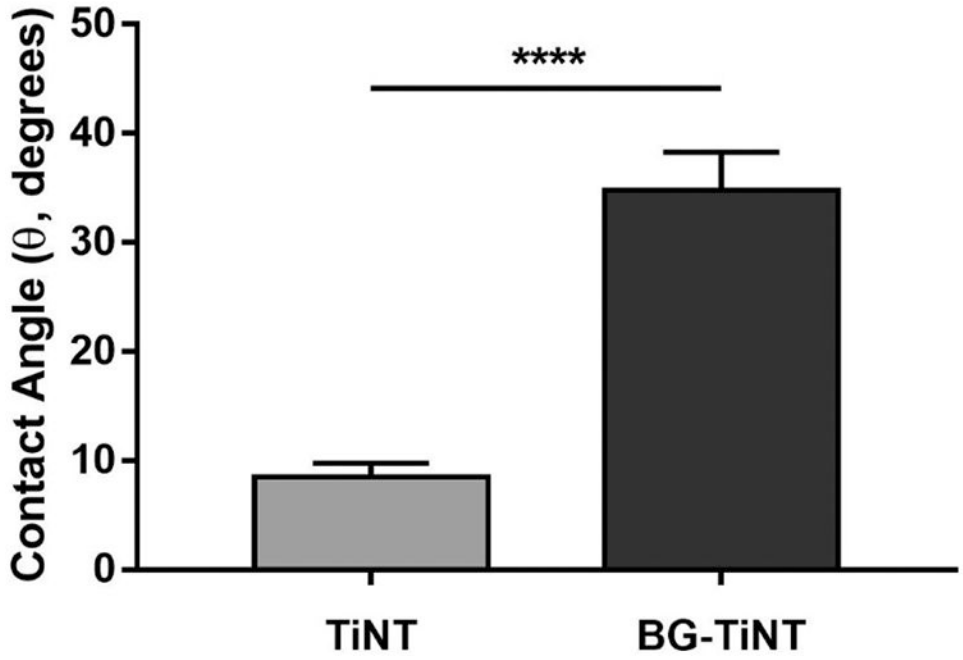

Fig. 3.

Apparent contact angles measured using DI water on TiNT and BG-TiNT. (****) indicates $p \leq 0.0001$.

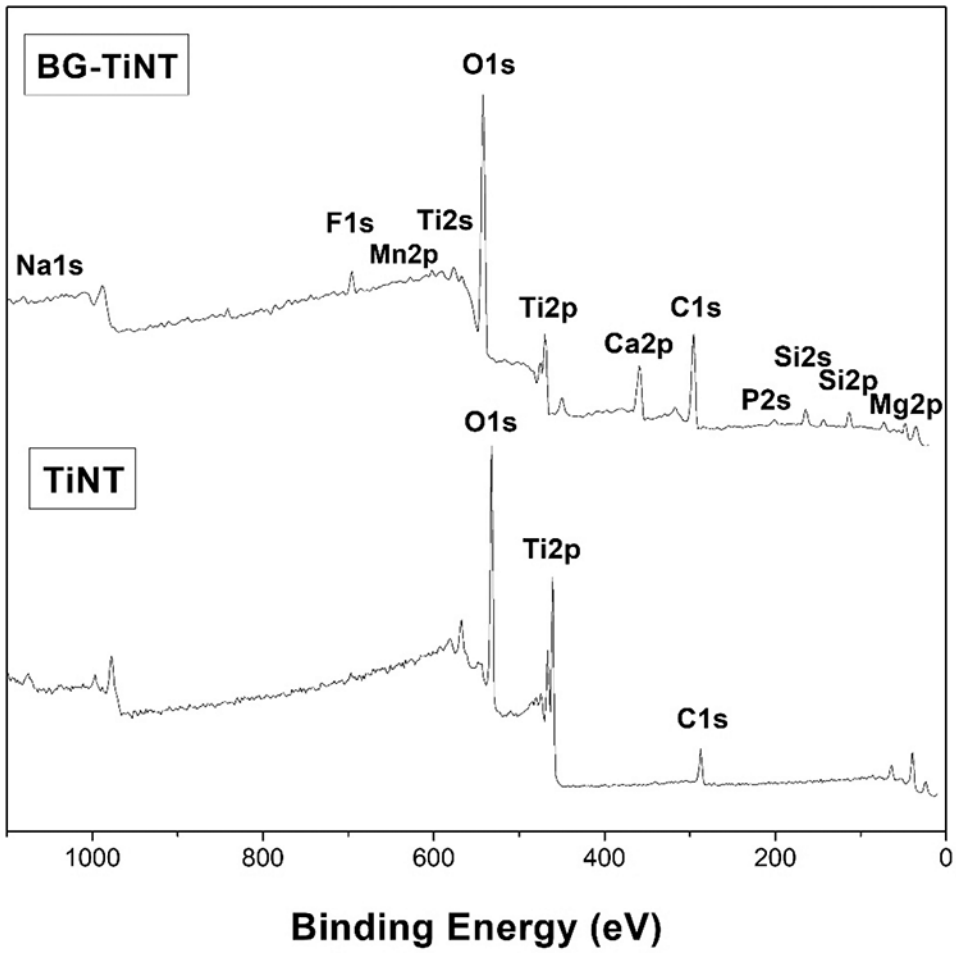

Fig. 4.
XPS survey scans of TiNT and BG-TiNT substrates.

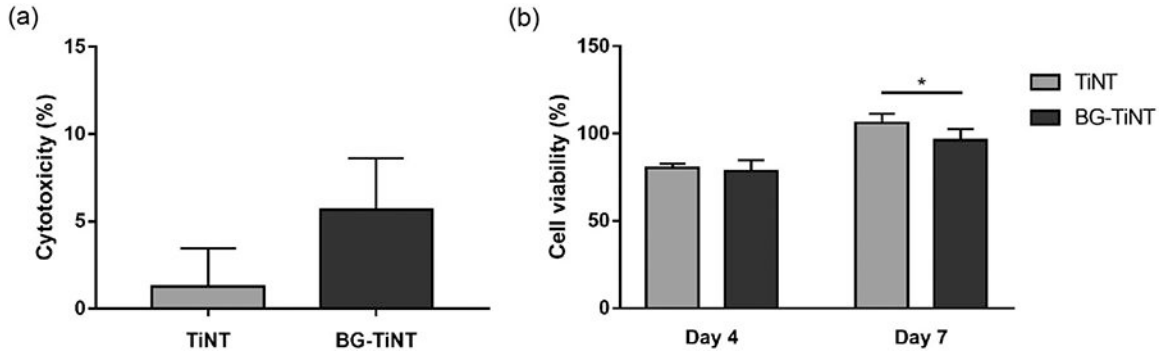

Fig. 5.

(a) Cytotoxicity of ADSCs exposed to both substrates after 1 day of cell culture. The results indicate no significant differences in the LDH activity between TiNT and BG-TiNT. (b) Cell viability of ADSCs exposed to both substrates measured using Alamar Blue assay (* indicates $p \leq 0.05$).

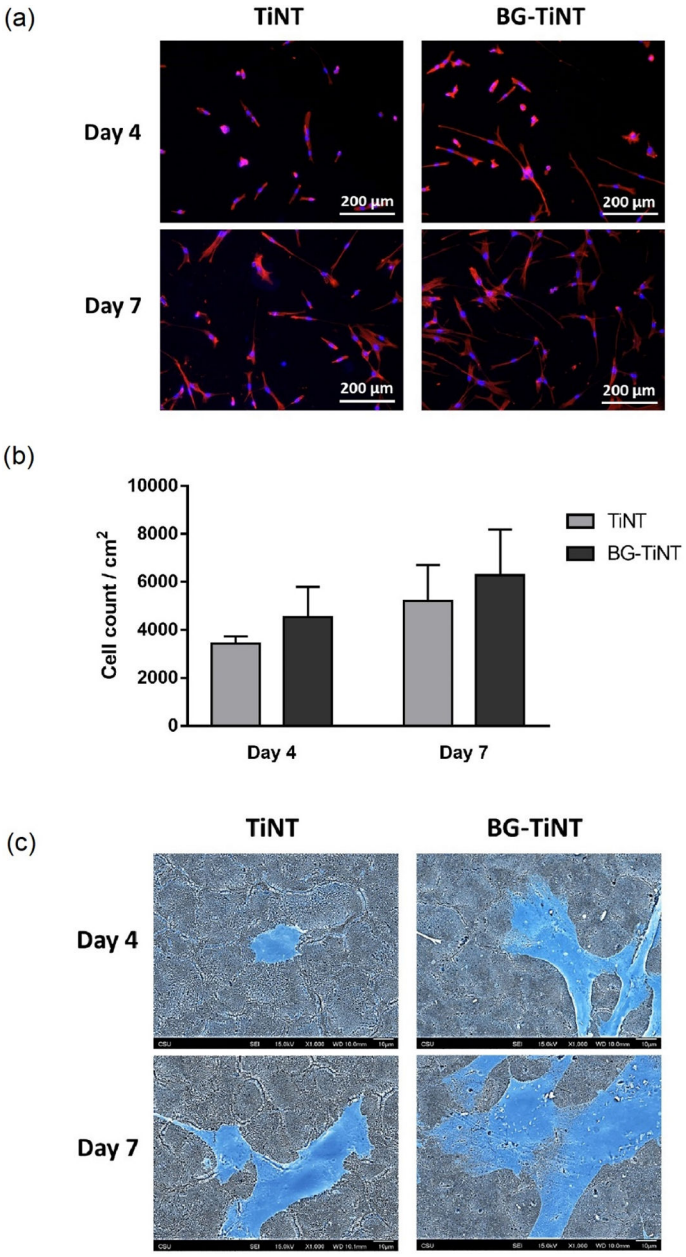

Fig. 6.

(a) Fluorescent images of ADSCs stained with rhodamine–phalloidin (red) and DAPI (blue) after 4 and 7 days of cell culture. (b) Cell count per cm^2 on TiNT and BG-TiNT calculated using ImageJ. The results indicate no significant differences in the number of cells adhered between the substrates. (c) Representative SEM images of adhered cells on TiNT and BG-TiNT. The images were taken at 1000X magnification. For a better visualization, the cells are post blue-colored.

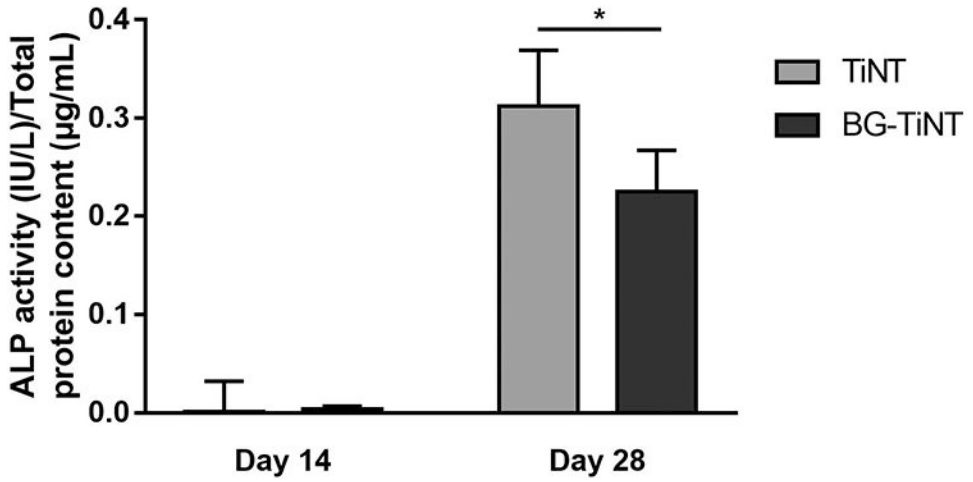

Fig. 7.

ALP activity of both substrates normalized by total protein content. TiNT shows significant higher ALP activity when compared to BG-TiNT after 28 days of cell culture (* indicates $p \leq 0.05$).

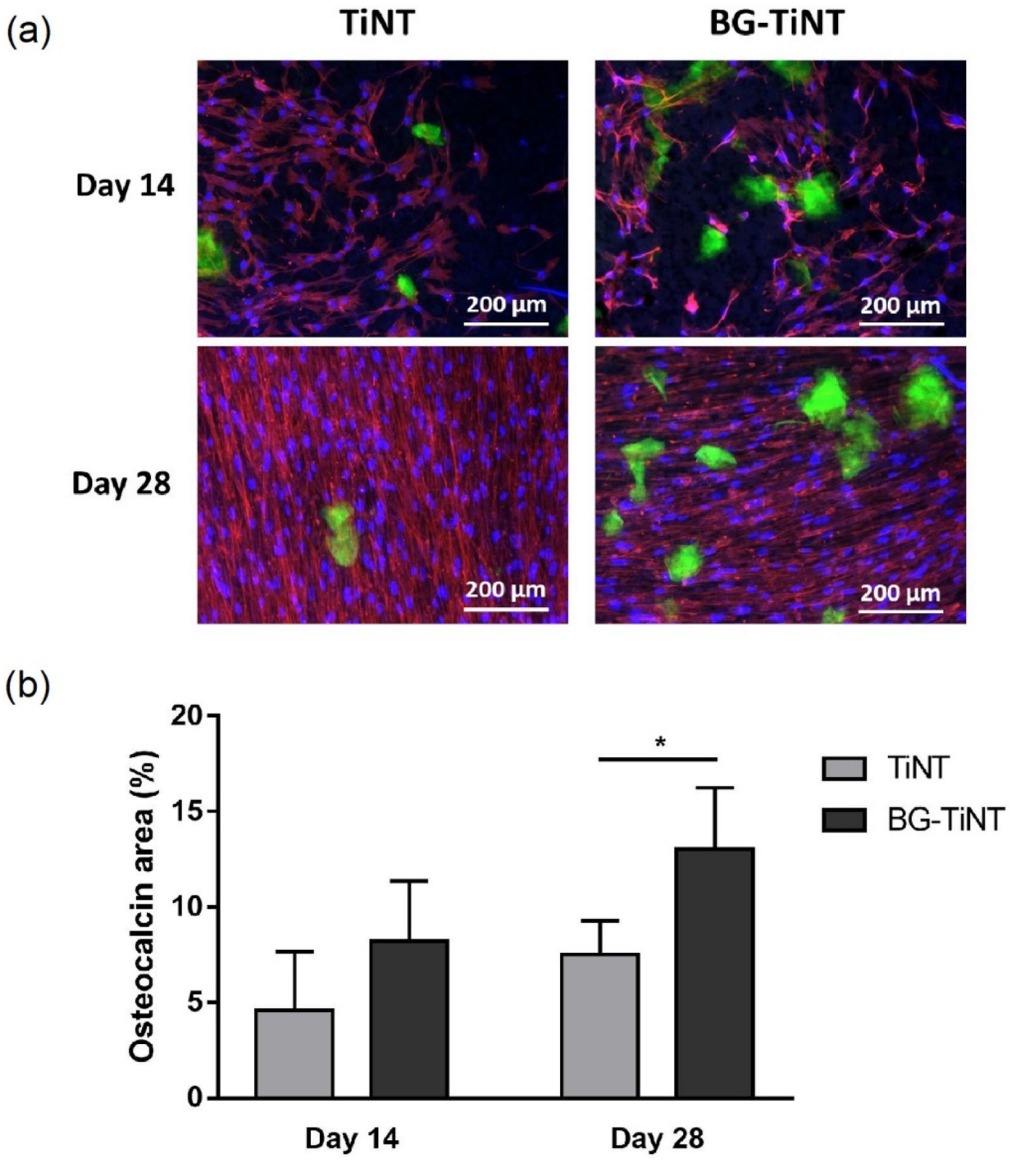

Fig. 8.

(a) Immunofluorescent images of ADSCs stained with rhodamine-phalloidin (red), DAPI (blue), and FITC for osteocalcin (green) on TiNT and BG-TiNT. (b) Percentage osteocalcin area after 14 and 28 days of cell culture calculated using ImageJ. BG-TiNT shows significant higher percentage area coverage than TiNT after 28 days (* indicates $p \leq 0.05$).

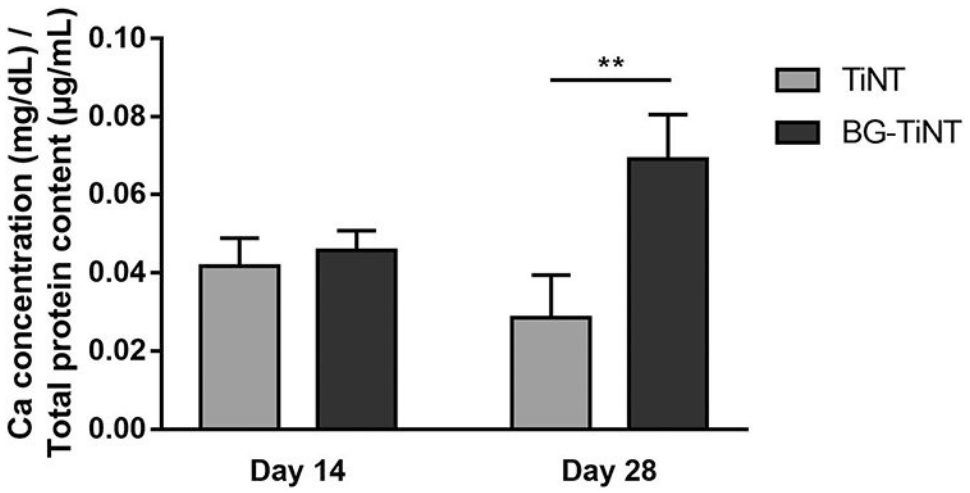

Fig. 9.

Calcium concentration on the substrates normalized by total protein content. BG-TiNT shows significant higher calcium content than TiNT after 28 days of cell culture (** indicates $p \leq 0.01$).

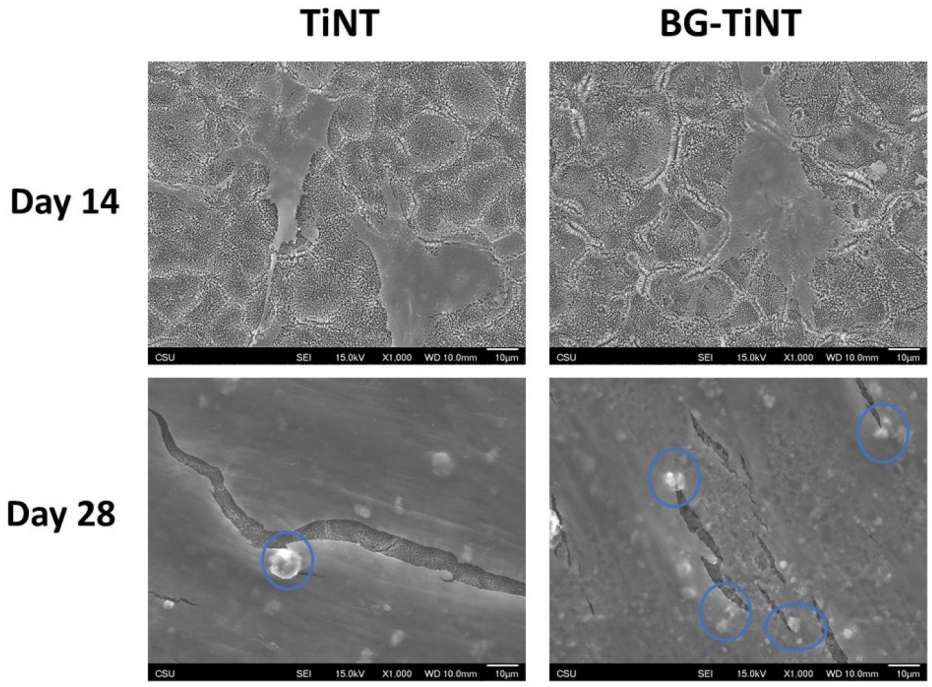

Fig. 10.

SEM images of ADSCs on the substrates after 14 and 28 days of cell culture. The images were taken at 1000X magnification.